Two-Stage Coordinated Robust Planning of Multi-Energy Ship Microgrids Considering Thermal Inertia and Ship Navigation

Nan Yang, *Senior Member*, *IEEE*, Guobin Xu, Zhineng Fei, *Student Member*, *IEEE*, Zhengmao Li*, *Senior Member*, *IEEE*, Liang Du, *Senior Member*, *IEEE*, Josep M. Guerrero, *Fellow IEEE*, Yuehua Huang, *Member*, *IEEE*, Jing Yan, Chao Xing, *Member*, *IEEE*, Zhenhua Li, *Senior Member*, *IEEE*

***Abstract*—**As maritime technology advances, multi-energy ship microgrids (MESMs) are widely used in large cruise tourism. In this context, studying cost-effective and highly reliable energy system planning methods for MESMs in their whole lifespan becomes paramount. Therefore, this paper proposes a joint planning method for a MESM during its lifespan. Firstly, a long timescale coordinated planning and operation scheme is formulated with the aim of maximizing the Net Present Value (NPV) value, thereby reducing both project investment and energy supply cost. In addition, this paper introduces novel operation models that incorporate customer thermal comfort levels, considering thermal inertia, and ship navigation, accounting for the effects of waves and wind. These models enhance the flexibility and practicality of the planning process. Finally, to ensure the safe operation of vessel and alleviate the negative effects of uncertain wind and waves during ship navigation, a robust optimization (RO) approach is employed. A case study demonstrates the effectiveness of the proposed method, with several comparison analyses further highlighting its advantages.**

***Index Terms*—planning and operation, multi-energy ship microgrids, robust optimization, thermal inertia, ship navigation.**

Nomenclature

Abbreviations

CCHP	Combined cooling heat and power
BT	Battery
PV	Photovoltaic
TS	Thermal storage
PtC	Power-to-thermal conversion
DGs	Diesel generators
GT	Gas turbine
WHB	Waste heat boiler
AC	Absorption cooling
EB	Electric boiler
EC	Electric cooling
KKT	Karush–kuhn–tucker
MESMs	Multi-energy ship microgrids
SP	Stochastic programming
RO	Robust optimization
NPV	Net present value
IRR	Internal Rate of Return
C&CG	Column-and-constraint generation
MILP	Mixed integer linear programming

Sets and Indices

I	Set of equipment
R_i / S_i	Set of installation capacity/ volume or area
k	Set of electrical, cooling, and heating loads
d	Set of generator
w	Set of weather
m	Set of heating and cooling loads

Parameters

$v^{\min}$ / $v^{\max}$	Minimum/maximum speed of the vessel
$\Phi_{\min}$ / $\Phi_{\max}$	Minimum/maximum distance traveled by the vessel
r_{wave} / r_{wind}	The resistance coefficient of waves/wind on ships
ρ_{water} / ρ_{air}	Sea water/air density
T_{in}^{min} / T_{in}^{max}	Minimum/maximum indoor temperature
$-\vartheta$ / ϑ	Minimum/maximum value of the PMV indicator
$p_{el,e}^{DG,\max}$ / $p_{el,e}^{GT,\max}$	Maximum output power of DGs/GT
$p_{el,h}^{WHB,\max}$ / $p_{el,c}^{AC,\max}$	Maximum output power of WHB/AC
$p_{el,h}^{EB,\max}$ / $p_{el,c}^{EC,\max}$	Maximum output power of EB/EC
$p_{el,e}^{PV,\max}$	Maximum output power of PV
$p_{el,e}^{DG,\min}$ / $p_{el,e}^{GT,\min}$	Minimum output power of DGs, GT
$p_{el,e,c}^{BT,\max}$ / $p_{el,e,d}^{BT,\max}$	Maximum charging/discharging power of BT

This paper was produced by the National Natural Science Foundation of China under Grant 62233006. (Corresponding author: Zhengmao Li.).

Nan Yang, Guobin Xu, Yuehua Huang and Zhenhua Li are with the College of Electrical Engineering and New Energy, China Three Gorges University, Yichang, China (e-mail:ynyyayy@ctgu.edu.cn; x18871136145@163.com;hyh@ctgu.edu.cn; lizhenhua1993@163.com).

Zhineng Fei and Zhengmao Li are with the school of Electrical Engineering, Aalto University, Finland (e-mail: zhineng.fei@aalto.fi and zhengmao.li@aalto.fi).

Liang Du is with the Department of Electrical and Computer Engineering, Temple Univerisity, Philadelphia, PA, United States (e-mail: ldu@temple.edu).

Josep M. Guerrero is with the Center for Research on Microgrids, Technical University of Catalonia, Spain (e-mail: josep.m.guerrero@upc.edu).

Jing Yan is with the State Grid Hubei Electric Power Co., Ltd. Economic and Technical Research Institute, Wuhan, China (e-mail: jason.yan@whu.edu.cn).

Chao Xing is with the Electric Power Research Institute, Yunnan Power Grid Company, Kunming, China (e-mail: 497336360@qq.com).

$p_{el,h,c}^{TS,\max}$ / $p_{el,h,d}^{TS,\max}$	Maximum storage/release power of TS
p_{ld}^{m}	*M*-type load
μ_{BT}^{loss} / $\mu_{TS,m}^{loss}$	Energy loss rate of BT/TS *m*-type energy
$\eta_{TS,m}^{c}$ / $\eta_{TS,m}^{d}$	Charging/discharging efficiency of *m*-type energy in TS
η_{BT}^{c} / η_{BT}^{d}	Charge and discharge efficiency of BT
R_{all} / R_c	Total resistance of vessel navigation/ resistance in still water
g	Gravitational acceleration
S_{wind}	Windward area of the vessel
α_{pl} / β_{pl}	Proportional/exponential coefficient in the relationship between ship propulsion loads and speed
v_o	Seawater flow rate
ΔT	Temperature difference for heating purposes
N_T	Total sailing time
H^a	Heat flux per unit area
S	Heating area
M	Human energy metabolism rate
μ^a	Heat loss per unit temperature difference
ΔT	Heating temperature difference
h_4 / h_5 / h_6	Constant coefficient
N_y	Project lifetime
T_{cl}	Thermal resistance of clothing worn by the human body
σ	Discount rate
δ_d^U	Unit start-up cost of the *d*-type unit
θ_{gas}	Heating value of natural gas
κ_{diesel} / κ_{gas}	Carbon emission cost coefficient for diesel/natural gas
ζ_d	Annual health decline rate of *d*-type equipment
λ_{DG} / λ_{GT}	Power generated by DG/GT's consumption per unit of diesel/ natural gas
η_{WHB} / η_{AC} / η_{EB}	Efficiency of WHB/AC/EB
η_{EC} / η_{PV}^{w}	Efficiency of EC/PV
η_{BT}^{c} / η_{BT}^{d}	Efficiency of EC/PV/BT charging/discharge
$\eta_{TS,m}^{c}$ / $\eta_{TS,m}^{d}$	Efficiency of TS charging/discharging
Δt	The unit dispatch period
n_i	Maximal allowable number of start-up and shut-down cycles for unit

Variables

v^t / v_c^t / v_o^t	Cruising speed/ cruising speed in calm water/ Seawater velocity
I_o^t	Directional relationship between ocean current and course of navigation
Φ_s^t	Vessel's cruising distance
p_{pl}^t	Propulsion load of the vessel
$T_{in}(t)$ / $T_{out}(t)$	Indoor and outdoor temperature
T_t	Average skin temperature of the human body under thermal comfort
C_P	Annual profit
C_d / C_v / C_g / C_c	Consumption/interruption penalty cost/gas consumption cost/carbon emissions cost
C_s / C_m / C_{age}	Start-up and shut-down/maintenance /health degradation cost
$P_{el,k}^{i,t}$	The *k*-type output of equipment *i*
U_d^t	Binary state of the *d*-type unit
$p_{el,e}^{DG,t}$ / $p_{el,e}^{GT,t}$	DG/GT output power
$p_{el,h}^{EB,t}$ / $p_{el,h}^{EC,t}$ / $p_{el,h}^{PV,t}$	Output power of EB/EC/PV
$p_e^{EB,t}$ / $p_e^{EC,t}$	Input power of EB/EC
$p_{el,e,c}^{BT,t}$ / $p_{el,e,d}^{BT,t}$	Charging/discharging power of BT
$p_{el,m,c}^{TS,t}$ / $p_{el,m,d}^{TS,t}$	*M*-type energy charging/discharging power of TS
$p_{ld}^{e,t}$ / $p_{ld}^{h,t}$ / $p_{ld}^{c,t}$	Electrical/thermal/cooling load of the system
$Q_e^{BT,t}$ / $Q_m^{TS,t}$	State of charge of BT/TS
h_t	Wave height
w_p^t	Wave period
θ_t	Wind direction angle
v_t^{wind}	Wind speed

I. Introduction

In recent years, the maritime transport industry has witnessed rapid growth, with multi-energy ships holding a significant share due to their higher operational flexibility and environmental friendliness [1]. In fact, those ships can be viewed as multi-energy ship microgrids (MESMs) since distributed generators, multi-energy loads, as well as heterogeneous energy storage systems are integrated [2]. According to [3], MESMs have substantial potential for cost savings and carbon emission reductions during their whole lifespan. Therefore, their optimal planning (investment) and operation (energy dispatch) are of great significance. In this light, how to jointly plan MESMs is now attracting increasing attention from both industrial and academic sectors.

The majority of current research efforts have focused on the effective operation of MESMs to achieve low-cost and emission goals. For example, Reference [4] proposed a two-stage multi-objective scheme to address the joint voyage scheduling and energy management problems by maximizing the provision of critical energy services and ensuring the safe ship return to the port under power shortage conditions. The study in [5] made full use of ship fleets as a potential maritime mobile microgrid for flexible scheduling to reduce the overall operational cost and greenhouse gas emissions. In [6]-[8], based on onshore electricity price forecasts, optimal ship scheduling, and power generation coordination were achieved to reduce energy supply costs and greenhouse gas

emissions. The study of [9] proposed energy conversion coupling models for various equipment, optimizing the scheduling of multiple diesel generators in MESMs using an improved particle swarm algorithm to smooth power fluctuations. However, the aforementioned studies are dedicated to short-term operations within a 24-hour timeframe, ignoring the MESM planning over longer timescales, such as 10 or 20 years.

To make optimal planning decisions for MESMs, a two-stage planning approach has been proposed to determine the capacity of carbon capture systems and the expansion capacity of energy storage systems, thereby reducing carbon emissions [10]. The study in [11] proposed the selection of a more suitable energy storage system for load-leveling actions based on wave periods and determined the dimensions of the storage system. To stabilize the ship's microgrid, an energy storage system (ESS) that combines supercapacitors (UC) and superconducting magnetic energy storage (SMES) is employed to reduce voltage disturbances resulting from dynamic load changes [12]. Additionally, economic and reliability issues arising from frequent load power disturbances in vessel propulsion systems can be addressed by proposing a composite energy device that integrates supercapacitors and batteries, optimized for capacity through a multi-objective optimization approach [13]. However, the above studies mainly focus on the planning of the energy storage system or other subsystems which is not enough for the whole ship system. In addition, current MESM planning methods simplify ship operations, disregarding the significant impact of environmental uncertainties on ship speed like wave and wind speed. Finally, the above works are limited to the ship's electrical energy management, neglecting multiple energy coordination between power and thermal (heating and cooling) energy [14]. This ignorance will hinder the economic operation of the MESM because thermal energy can bring extra flexibility given the thermal inertia, that is, humans can remain comfortable with slight indoor temperature variations from the ideal setting.

Additionally, for uncertainty handling: in the MESM, the propulsion load constitutes a significant portion of its operational load, which is directly related to the vessel's navigational speed. However, the uncertain wave and wind speed will greatly impact vessel speeds and further operational reliability. Therefore, addressing uncertainties becomes imperative to ensure the reliable operation of the MESM. Some previous studies have tried to address this challenge. In [15]-[16], the stochastic programming (SP) method is used to deal with uncertainties from loads and solar generations. Nevertheless, for one thing, they still are confined to the operational level, overlooking the impact of uncertainties on long-term planning. Moreover, the SP method typically involves taking expectations of stochastic parameters with known probability distributions. However, their solutions are too optimistic which is not suitable for ship operations where customer safety in any case is the priority [17]. Conversely, the robust optimization (RO) method, which ensures the feasibility of any system operation under the worst-case scenario can therefore be applied [18] for the MESM.

Given the above insights, this paper proposes a two-stage coordinated robust planning method for the MESM considering uncertain ship navigation and thermal inertia. The main contributions of this paper are summarized:

1) A two-stage coordinated planning method for the whole MESM is proposed. The optimal size of onboard generators, and energy storage systems is decided in a long timescale. This would highly contribute to reducing ship investment costs.

2) The ship navigation and thermal loads are practically modeled with the impacts of wave and wind speed as well as the thermal inertia. In this way, the ship operation is more practical and comprehensive.

3) To ensure the safety of ship operations and onboard customers, the RO method is used to handle the diverse uncertainties during ship navigation.

The rest of this paper is organized as follows: Section II presents the modeling of MESM and Section III proposes the formulation of the MESM planning model. Section IV introduces the solution method for uncertainty hedging; Section V presents a case study; Section VI summarizes the conclusions and future work.

II. System Modelling

A. Configuration of Multi-energy Ship Microgrids

The typical structure of a MESM embedded with the energy conversion blocks is shown in Fig.1. It consists of the combined cooling, heating, and power (CCHP) unit, heterogeneous energy storage (battery (BT), and Thermal storage (TS), photovoltaic (PV) system, power-to-thermal conversion (PtC) unit, diesel generators (DGs), and bidirectional converters. Additionally, the onshore power supply, known as "cold ironing" [6], has been incorporated to provide energy to the MESM when the ship berths at the port.

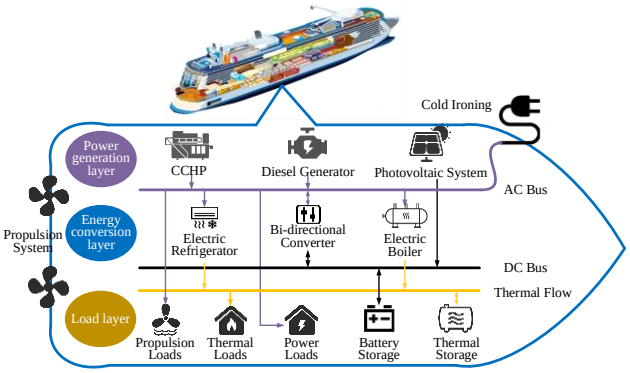

Fig. 1. The typical structure of the MESM.

In the MESM, the thermal energy is generated by the CCHP and PtC units. The primary sources of electrical energy are DGs, CCHP units, and PV systems. DGs combust diesel for power generation, and CCHP units consume natural gas, concurrently producing electricity, and TS for onboard multi-energy service demands. The BT, TS, and PtC units can enhance overall system flexibility and efficiency through energy storage, release, and conversion. Finally, all onboard

units are interconnected with their respective AC or DC buses, linked through bidirectional converters [18]-[20].

On the consumption side, electrical loads comprise the propulsion load, which is highly dependent on cruising speeds, and onboard electricity demands. Additionally, the onboard thermal loads are mainly from space heating or cooling.

B. Ship Voyage Modeling

The ship voyage includes cruising periods and berthing periods as shown in Fig. 2. During most cruising periods, the ship cruises at full speed, while for periods when it just approaches and departs from certain ports, it cruises at partial speed; during the berthing period, the shipping speed is strictly zero [21].

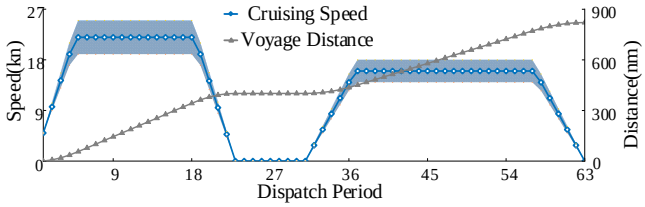

Fig. 2. Ship voyage pattern.

To ensure a punctual and safe voyage, the constraints for the voyage scheduling are:

1) The velocity of the ship must be maintained within prescribed upper and lower bounds to ensure the safety of navigation (1):

$$v^{\min} \le v^t \le v^{\max} \tag{1}$$

2) In our established case study, the vessel navigates through the Strait of Malacca, where ocean currents flow consistently from southeast to northwest throughout the year [22][23]. The ship's cruising distance is the accumulation of cruising speed over the corresponding time as denoted in (2). Concurrently, vessels must also ensure timely arrival at ports, as illustrated in (3):

$$\Phi_s^t = \Phi_s^{t-1} + \left(v^t + v_o^t \mathrm{I}_o^t\right)\Delta t \tag{2}$$

$$\Phi_{\min}^t \le \Phi_s^t \le \Phi_{\max}^t \tag{3}$$

3) The power consumption of the propulsion motor is a part of the electrical load, and its modeling is as (4)[24]:

$$p_{pl}^t = \left(\alpha_{pl} v_c^t\right)^{\beta_{pl}} R_{all} / R_c \tag{4}$$

where p_{pl}^t is a part of $p_{ld}^{e,t}$ in formula (29).

C. Ship Navigation Modelling

In maritime navigation, wind and waves are the most significant factors affecting vessel speed, as illustrated in Fig.3. in this context, the variables of wave height, wave period, wind direction angle, and wind speed are considered uncertain. It is further assumed that the direction of the waves aligns with the direction of the wind.

The resistance generated by waves and wind is shown in (5)-(6) [24]:

$$\Delta R_{wave} = \rho_{water} g h_t^2 r_{wave} w_p^t v_o \cos\theta_t \tag{5}$$

$$\Delta R_{wind} = \rho_{air} r_{wind} S_{wind} \left[\left(v_t^{wind} \cos\theta_t + v_c^t\right)^2 - \left(v_c^t\right)^2\right] \tag{6}$$

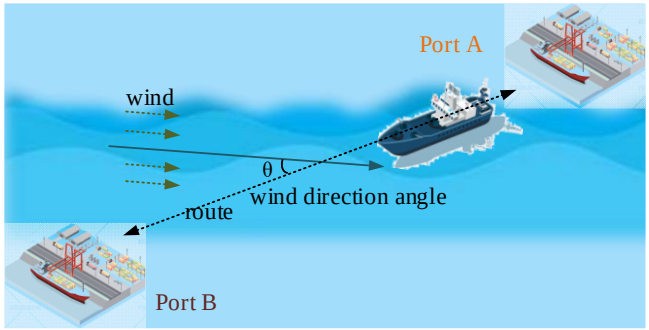

Fig. 3. The impact of uncertainty on ships during navigation.

The total resistance received by the ship is shown in (7)

$$R_{all} = R_c + \Delta R_{wave} + \Delta R_{wind} \tag{7}$$

D. The Thermal Inertia and Comfort Model of The Heating System.

The model for thermal inertia in heating/cooling zones within the ship is as Fig 4:

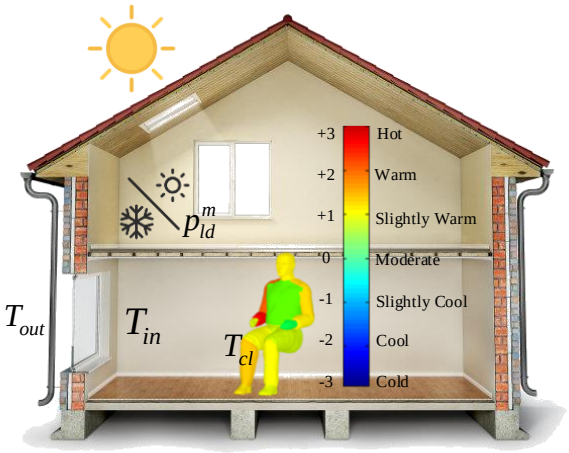

Fig. 4. Typical structure of a room in a MESM.

In enclosed spaces, thermal systems retain a relatively comfortable temperature for a period even after the thermal energy supply stops [25]. Moreover, human perception of thermal comfort has a lag. This is called the thermal inertia under which thermal loads can be regarded as an extra flexibility resource. The Predicted Mean Vote (PMV) index [26] which is a commonly used criterion for quantifying the thermal loads in a building is applied in this study. Satisfying human comfort, the model allows adaptive adjustment of thermal loads, thereby improving the MESM flexibility.

Table I
THE COMFORT LEVEL INDICATORS BASED ON PMV

Sensation	Hot	Warm	Slightly Warm	Moderate	Slightly Cool	Cool	Cold
Value	+3	+2	+1	0	-1	-2	-3

The current PMV index adopts a 7-point scale, as illustrated in Table I. A PMV value of 0 indicates the optimal thermal comfort state for the human body, when the PMV index fluctuates within the range of ±0.5, users do not perceive significant temperature differences. Model (8) is employed for the thermal inertia of the heating area.

$$\begin{cases} h_3 T_{in}(t) - T_{in}(t-1) = h_1 p_{ld}^{h,t} + h_2 T_{out}(t) \\ h_1 = \Delta T / H^a S \\ h_2 = \mu^a \Delta T / H^a \\ h_3 = 1 + h_2 \\ \Delta T = T_{in}(t) - T_{out}(t) \end{cases} \tag{8}$$

The relationship between the PMV index and the ambient temperature of the heating area is described in (9).

$$\lambda_{\mathrm{PMV}} = h_4 - \frac{h_5\left(T_t - T_{in}(t)\right)}{M\left(T_{cl} + h_6\right)} \tag{9}$$

The indoor temperature and PMV constraints are (10):

$$\begin{cases} T_{in}^{min} \le T_{in}(t) \le T_{in}^{max} \\ -\vartheta \le \lambda_{PMV} \le \vartheta \end{cases} \tag{10}$$

III. Problem Formulation

A. Two-Stage Planning Model

This paper proposes a two-stage optimization model as Fig.5 to coordinate all the decision variables.

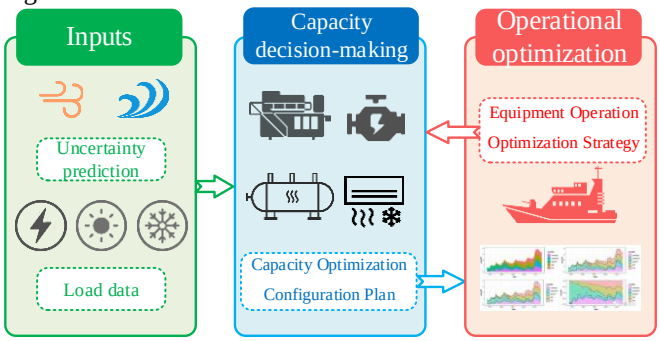

Fig. 5. Structure of MESM two-stage planning model.

Specifically, the first-stage problem determines the optimal configuration of all units in the MESM. The related costs for the whole planning scheme are the investment costs and operational costs. Meanwhile, the second stage is tasked with determining the optimal output of these units, with the objective function including costs related to fuel consumption, carbon emissions, interruption penalties, unit startup and shutdown, equipment maintenance, and degradation of equipment health and lifespan.

Net present value (NPV) is the difference between the present value of cash inflows and the present value of cash outflows over a period of time. NPV is used in capital budgeting and investment planning to analyze a project's projected profitability [27]. When the NPV equals 0, the corresponding discount rate is the Internal Rate of Return (IRR) value [28]. The specific planning model for individual systems is as follows:

$$NPV = \max_{z \in F_z, x \in G_x} \left\{ -F(z) + \sum_{t=1}^{N_y} \frac{C_p - G(x)}{(1+\sigma)^t} \right\} \tag{11}$$

$$s.t.\ \ F(z) = \sum_{i=DG}^{I} \left(C_i R_i\right) \tag{12}$$

$$G(x) = (C_d + C_v + C_g + C_c + C_s + C_m + C_{age}) \tag{13}$$

$$C_d = \sum_{t=1}^{T} \left(V_{diesel}^t C_{diesel}\right) \tag{14}$$

$$C_v = \sum_{t=1}^{T} \left(C_{k,voll}^t P_{k,voll}^t\right) \tag{15}$$

$$C_g = \sum_{t=1}^{T} \left(V_{gas}^t C_{gas}\right) \tag{16}$$

$$C_c = \sum_{t=1}^{T} \left(\kappa_{diesel} V_{diesel}^t + \kappa_{gas} V_{gas}^t\right) \tag{17}$$

$$C_s = \sum_{t \in T} \max\left\{0, U_d^t - U_d^{t-1}\right\} \delta_d^U, d \in \{GT, DG\} \tag{18}$$

$$C_m = \sum_{i=DG}^{I} \sum_{t=1}^{T} \left(C_{main}^i p_{el,k}^{i,t}\right) \tag{19}$$

$$C_{age} = \sum_{D \in \{BT,PV\}} \zeta_D y C_D R_D \tag{20}$$

$$I \in \{DG, GT, WHB, AC, EB, EC, PV, BT, TS\} \tag{21}$$

In Equation (11), z represents the decision variable during the planning phase, which includes the types, sizes, and capacities of the equipment. C_p represents the annual revenue, which we treat as a fixed value. Calculations use a 109% [29] annual occupancy rate for the cruise ship to compare the NPV and IRR values across different methods. F_z denotes the constraints on equipment planning, as shown in (30)–(31), while F_z refers to the objective in the investment phase. x represents the decision variables during the operational phase, such as fuel consumption, gas consumption, load shedding, the number of start-stop cycles, and equipment lifespan degradation. G_x and $G(x)$ represent the constraints and objectives in the operational phase, respectively. Equation (12) denotes the investment cost; (13) refers to the operational cost; (14) corresponds to fuel consumption cost; (15) represents the interruption penalty cost; (16) refers to gas consumption cost; (17) denotes the carbon emission cost; (18) represents the start-up and shut-down costs of the units; (19) refers to maintenance costs; (20) represents equipment degradation costs; and (21) defines the equipment set.

B. Equality Constraints

Eq (22) represents the consumption of natural gas and diesel; (23) serves as a constraint for energy conversion devices; (24) represents the output of photovoltaics; (25) and (26) depict the outputs of electric, thermal, and cooling energy storage; (27) and (28) indicate the coexistence and storage capability of electric, thermal, and cooling energy storage systems; (29) denotes the energy conversion module.

$$\begin{cases} V_{diesel}^t(p) = p_{el,e}^{DG,t} / \lambda_{DG} \\ V_{gas}^t(p) = \begin{cases} p_{el,e}^{GT,t} / \lambda_{gt} \\ p_{el,h}^{WHB,t} / \eta_{WHB} \theta_{gas} \\ p_{el,h}^{AC,t} / \eta_{AC} \theta_{gas} \end{cases} \end{cases} \tag{22}$$

$$\begin{bmatrix} p_{el,h}^{EB,t} \\ p_{el,c}^{EC,t} \end{bmatrix} = \begin{bmatrix} \eta_{EB}\left(1 - \mu_{EB}^{loss}\right) & 0 \\ 0 & \eta_{EC} \end{bmatrix} \begin{bmatrix} p_e^{EB,t} \\ p_e^{EC,t} \end{bmatrix} \tag{23}$$

$$S_{PV} = p_{el,e}^{PV,t} / \eta_{PV}^w I_G^t, w \in \{\text{clear/cloudy/rainy day}\} \tag{24}$$

$$Q_e^{BT,t}=\left(1-\mu_{BT}^{loss}\right)Q_e^{BT,t-1}+\left(\eta_{BT}^{c}p_{el,e,c}^{BT,t}-p_{el,e,d}^{BT,t}/\eta_{BT}^{d}\right)\Delta t/S_{BT} \tag{25}$$

$$p_{el,e,c}^{BT,t}p_{el,e,d}^{BT,t}=0,\forall t\in N_T \tag{26}$$

$$\begin{cases} Q_m^{TS,t+1}=(1-\mu_{TS,m}^{loss})Q_m^{TS,t}+ \\ \qquad (\eta_{TS,m}^{c}p_{el,m,c}^{TS,t}-p_{el,m,d}^{TS,t}/\eta_{TS,m}^{d})\Delta t/S_h \\ m\in\{h,c\} \end{cases} \tag{27}$$

$$p_{el,h,c}^{TS,t}p_{el,h,d}^{TS,t}=0,\forall t\in N_T \tag{28}$$

$$\begin{bmatrix} p_{ld}^{e,t} \\ p_{ld}^{h,t} \\ p_{ld}^{c,t} \end{bmatrix}=\begin{bmatrix} p_{el,e}^{DG,t} & p_{el,e}^{GT,t} & p_{el,e}^{PV,t} & p_{el,e,d}^{BT,t} \\ p_{el,h}^{WHB,t} & p_{el,h}^{EB,t} & p_{el,h,d}^{TS,t} & 0 \\ p_{el,h}^{AC,t} & p_{el,c}^{EC,t} & p_{el,c,d}^{TS,t} & 0 \end{bmatrix}\begin{bmatrix} 1 \\ 1 \\ 1 \\ 1 \end{bmatrix} \tag{29}$$

C. Inequality Constraints

The installation capacity, volume, and spatial constraints of the equipment are as follows:

$$0\le R_I\le R_I^{\max} \tag{30}$$

$$0\le S_I\le S_I^{\max} \tag{31}$$

The constraints on the output limits of the devices are illustrated as (32)-(37):

$$\sum_{t=1}^{T}\left|U_d^t-U_d^{t-1}\right|\le n_i \tag{32}$$

$$p_{el,e}^{DG,\min}\le p_{el,e}^{DG,t}\le p_{el,e}^{DG,\max} \tag{33}$$

$$p_{el,e}^{GT,\min}\le p_{el,e}^{GT,t}\le p_{el,e}^{GT,\max} \tag{34}$$

$$\left[p_{el,h}^{WHB,t},p_{el,h}^{AC,t},p_{el,h}^{EB,t}\right]\begin{cases}\ge[0,0,0] \\ \le\left[p_{el,c}^{WHB,\max},p_{el,c}^{AC,\max},p_{el,h}^{EB,\max}\right]\end{cases} \tag{35}$$

$$\left[p_{el,c}^{EC,t},p_{el,e}^{PV,t},p_{el,e,c}^{BT,t}\right]\begin{cases}\ge[0,0,0] \\ \le\left[p_{el,c}^{EC,\max},p_{el,e}^{PV,\max},p_{el,e,c}^{BT,\max}\right]\end{cases} \tag{36}$$

$$\left[p_{el,e,d}^{BT,t},p_{el,h,c}^{TS,t},p_{el,h,d}^{TS,t}\right]\begin{cases}\ge[0,0,0] \\ \le\left[p_{el,e,d}^{BT,\max},p_{el,h,c}^{TS,\max},p_{el,h,d}^{TS,\max}\right]\end{cases} \tag{37}$$

IV. Solution Methodology

A. Compact Form of Two-stage Planning Model

The two-stage planning problem of MESM is rephrased in a compact form:

$$\min_{\mathbf{x},\mathbf{y}}\ \mathbf{c}^{\mathbf{T}}\mathbf{y}+\mathbf{b}^{\mathbf{T}}\mathbf{x} \tag{38}$$

$$s.t.\ \ \mathbf{y}\in\mathbf{d} \tag{39}$$

$$\mathbf{Gx}\ge\mathbf{h}-\mathbf{Ey}-\mathbf{Mu},\ \mathbf{u}\in\Omega \tag{40}$$

$$\mathbf{S}_{\mathbf{y}}\subseteq\mathbf{R}_{+}^{\mathbf{n}} \tag{41}$$

$$\mathbf{S}_{\mathbf{x}}\subseteq\mathbf{R}_{+}^{\mathbf{m}} \tag{42}$$

The first-stage optimization problem optimizes the equipment capacity configuration before the realization of uncertainties, where $\mathbf{c}^{\mathbf{T}}\mathbf{y}$ denotes the investment costs, the vector $\mathbf{y}$ represents the relevant variables: R_{DG}, R_{GT}, R_{WHB}, R_{AC}, R_{EC}, R_{EB}, R_{PV}, R_{BT}, R_{TS}, corresponding formulas (12); where $\mathbf{d}$ represents the feasible region represented by formula (30)-(31). The second-stage optimization problem optimizes the equipment output under uncertainty, where $\mathbf{b}^{\mathbf{T}}\mathbf{x}$ represents the operating costs, the vector $\mathbf{x}$ represents the remaining continuous variables: V_{diesel}^t, V_{gas}^t, $P_{k,voll}^t$, $p_{el,k}^{j,t}$, and discrete variable: U_d^t, $\mathbf{u}$ represents the relevant parameters of the second-stage decision variables, which are uncertain. Formulas (41)-(42) represent nonnegative decision variables where $\mathbf{x}$ and $\mathbf{y}$ are $n\times1$ and $m\times1$ dimensions, respectively.

Given the two-stage planning framework in Section III-A, the two-stage RO model can be expressed as:

$$\min_{\mathbf{y}}\ \mathbf{c}^{\mathbf{T}}\mathbf{y}+\max_{\mathbf{u}\in\Omega}\ \boldsymbol{\eta}(\mathbf{y},\mathbf{u}) \tag{43}$$

$$s.t.\ \ \mathbf{y}\in\mathbf{d} \tag{44}$$

$$\boldsymbol{\Gamma}(\mathbf{y},\mathbf{u})\ne\varnothing,\ \ \forall\mathbf{u}\in\Omega \tag{45}$$

$$\eta(y,u)\coloneqq\min_{\mathbf{x}\in\boldsymbol{\Gamma}(\mathbf{y},\mathbf{u})}\mathbf{b}^{\mathbf{T}}\mathbf{x} \tag{46}$$

$$\boldsymbol{\Gamma}(\mathbf{y},\mathbf{u})\coloneqq\{\mathbf{Gx}\ge\mathbf{h}-\mathbf{Ey}-\mathbf{Mu}\} \tag{47}$$

Here, the uncertainties associated with wind, wave, photovoltaic output, and outdoor temperature are considered as a set. Formulas (46)-(47) represent the optimization of second-stage operations under given uncertainty scenarios $\mathbf{u}$, with first-stage decisions $\mathbf{y}$ and constraints $\boldsymbol{\Gamma}(\mathbf{y},\mathbf{u})$, replacing the predicted load $\mathbf{h}$ to derive the second-stage cost $\boldsymbol{\eta}(\mathbf{y},\mathbf{u})$. Subsequently, (43) yields the uncertainty scenarios that maximize the minimum value of $\boldsymbol{\eta}(\mathbf{y},\mathbf{u})$ under given first-stage decisions $\mathbf{y}$. Consequently, the robust program can identify solutions that minimize first-stage costs while mitigating worst-case second-stage costs.

To solve the RO model incorporating uncertainty parameters, comprehensive modeling of all uncertain parameters is undertaken. In this study, the column-and-constraint generation (C&CG) algorithm, which solves the problem by changing the robust model into the master and slave problems, is utilized [30].

B. Uncertain Sets Modelling

The overall uncertainty set is shown below:

$$\Omega=\left\{\begin{array}{l} u_j^{\min}\le u_j^t\le u_j^{\max},\forall t\in N_T \\ \underline{\mu}^{u_j}\le\sum_{t\in N_T}u_j/\sum_{t\in N_T}\bar{u}_j\le\bar{\mu}^{u_j}\end{array}\right\} \tag{48}$$

where u_j represents the uncertainty parameters of wind direction, wind speed, wave height, wave period, photovoltaic power generation, outdoor temperature, and service load., while $\bar{\mu}$ and $\underline{\mu}$ denote the upper and lower budgets of the uncertainty set. In the uncertainty set, the actual uncertain value can vary between the lower ($u_j^{\min}$) and upper limits ($u_j^{\max}$), while the overall variation is controlled by the user-defined lower ($\underline{\mu}^{u_j}$) and upper ($\bar{\mu}^{u_j}$) budget levels.

The uncertain operation model of MESM can be written in the following form:

$$\min \ \mathbf{c}^{\mathrm{T}}\mathbf{y} + \max_{\mathbf{u}\in\Omega} \ \min_{\mathbf{x}\in\Gamma(\mathbf{y},\mathbf{u})} \mathbf{b}^{\mathrm{T}}\mathbf{x} \tag{49}$$

$$s.t. \ \ \mathbf{y} \in \mathbf{d} \tag{50}$$

$$\mathbf{Gx} \geq \mathbf{h} - \mathbf{Ey} - \mathbf{Mu}, \ \mathbf{u} \in \Omega \tag{51}$$

$$\mathbf{S}_{\mathbf{y}} \subseteq \mathbf{R}_{+}^{\mathbf{n}} \tag{52}$$

$$\mathbf{S}_{\mathbf{x}} \subseteq \mathbf{R}_{+}^{\mathbf{m}} \tag{53}$$

C. Master Problem

To solve this model using the C&CG method, it is necessary to decompose it into the following master problem:

$$\min \ \mathbf{c}^{\mathrm{T}}\mathbf{y} + \boldsymbol{\eta} \tag{54}$$

$$s.t. \ \ \mathbf{y} \in \mathbf{d} \tag{55}$$

$$\boldsymbol{\eta} \geq \mathbf{b}^{\mathrm{T}}\mathbf{x}_j, \quad j = 1,...,r \tag{56}$$

$$\mathbf{Ey} + \mathbf{Gx}_j \geq \mathbf{h} - \mathbf{Mu}_j, \quad j = 1,...,r \tag{57}$$

$$\mathbf{y} \in \mathbf{S}_{\mathbf{y}} \tag{58}$$

$$\mathbf{x}_j \in \mathbf{S}_{\mathbf{x}}, \quad j = 1,...,r \tag{59}$$

Due to the linear nature of the constraints in the master problem, it constitutes a Mixed Integer Linear Programming (MILP) problem.

D. Subproblem

The subproblem is as follows:

$$\max_{\mathbf{u}\in\Omega} \ \min_{\mathbf{x}\in\Gamma(\mathbf{y},\mathbf{u})} \mathbf{b}^{\mathrm{T}}\mathbf{x} \tag{60}$$

$$s.t. \ \ \mathbf{Gx} \geq \mathbf{h} - \mathbf{Ey} - \mathbf{Mu}, \ \ \mathbf{u} \in \Omega \tag{61}$$

$$\mathbf{S}_{\mathbf{x}} \subseteq \mathbf{R}_{+}^{\mathbf{m}} \tag{62}$$

Because the objective function and constraint conditions of the subproblem are continuously differentiable, the KKT condition can be used. By using KKT conditions [31] for transformation, the subproblem can be transformed into:

$$\max_{\mathbf{u}\in\Omega} \mathbf{b}^{\mathrm{T}}\mathbf{x} \tag{63}$$

$$s.t. \ \ \mathbf{Gx} \geq \mathbf{h} - \mathbf{Ey} - \mathbf{Mu}, \ \ \mathbf{u} \in \Omega \tag{64}$$

$$\mathbf{G}^{\mathrm{T}}\boldsymbol{\pi} \leq \mathbf{b} \tag{65}$$

$$\left(\mathbf{Gx} - \mathbf{h} - \mathbf{Ey} - \mathbf{Mu}\right)_i \boldsymbol{\pi}_i = 0, \ \ \mathbf{u} \in \Omega, \forall i \tag{66}$$

$$\left(\mathbf{b} - \mathbf{G}^{\mathrm{T}}\boldsymbol{\pi}\right)_{\mathbf{l}} \mathbf{x}_{\mathbf{l}} = 0, \ \ \forall l \tag{67}$$

$$\mathbf{x} \geq 0 \tag{68}$$

$$\boldsymbol{\pi} \geq 0 \tag{69}$$

By equivalently linearizing the subproblem, it transforms into:

$$\max_{\mathbf{u}\in\Omega} \mathbf{b}^{\mathrm{T}}\mathbf{x} \tag{70}$$

$$s.t. \ \ \mathbf{Gx} \geq \mathbf{h} - \mathbf{Ey} - \mathbf{Mu}, \ \ \mathbf{u} \in \Omega \tag{71}$$

$$\mathbf{G}^{\mathrm{T}}\boldsymbol{\pi} \leq \mathbf{b} \tag{72}$$

$$\boldsymbol{\pi}_i \leq \mathbf{M}\boldsymbol{\varsigma}_i, \ \ \forall i \tag{73}$$

$$\left(\mathbf{Gx} - \mathbf{h} - \mathbf{Ey} - \mathbf{Mu}\right)_i \leq \mathbf{M}\left(1 - \boldsymbol{\varsigma}_i\right), \ \ \forall i \tag{74}$$

$$\mathbf{x}_i \leq \mathbf{M}\boldsymbol{\omega}_i, \ \ \forall i \tag{75}$$

$$\left(\mathbf{b} - \mathbf{G}^{\mathrm{T}}\boldsymbol{\pi}\right)_l \leq M\left(\mathbf{1} - \boldsymbol{\omega}_l\right), \ \ \forall l \tag{76}$$

$$\mathbf{x} \geq 0 \tag{77}$$

$$\boldsymbol{\pi} \geq 0 \tag{78}$$

$$\boldsymbol{\xi}, \boldsymbol{\omega} \in \{0,1\}^n \tag{79}$$

Thus, the subproblem also becomes a MILP problem following this transformation.

V. Case Studies

A. Test System.

The route of MESM is illustrated in Fig. 6. DGs, CCHP, PV, energy conversion units, and storage systems are harmonized to propel this voyage. This cruise liner is designed for entertainment and sightseeing purposes, with a tonnage of 169,379 tons and a capacity of 5,549 passengers. Departing from Singapore (Port A) at 5:00 PM, the vessel arrives at Penang, Malaysia (Port B) the following day at 3:00 PM, staying until 11:00 PM before departing again. Finally, it returns to Singapore (Port A) at 7:00 AM on the fourth day. The average number of rainy days in the vessel's navigation area is 139 days per year, while cloudy days account for 80 days, and sunny days total 146 days annually [32]. The planned lifespan is 15 years.

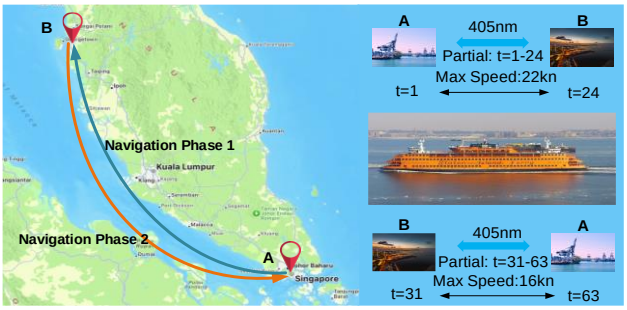

Fig. 6. Navigation route for the test MESM.

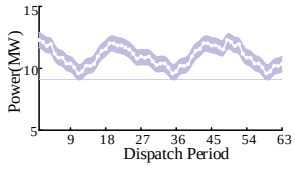

(a) Electricity load prediction

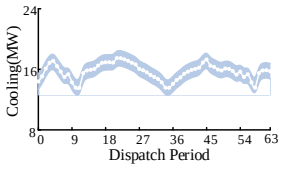

(b) Cooling load prediction

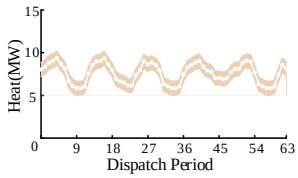

(c) Heat load prediction

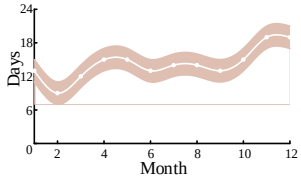

(d) Non sunny days prediction

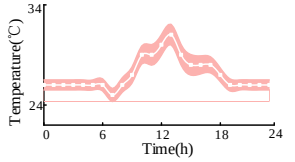

(e) Outdoor temperature prediction

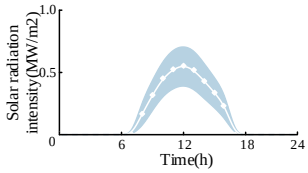

(f) Solar irradiance intensity prediction (clear day)

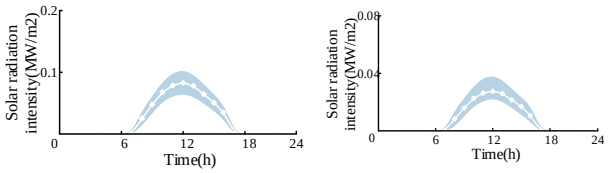

(g) Solar irradiance intensity prediction (cloudy day) (h) Solar irradiance intensity prediction (rainy day)

Fig. 7. Interval predictions for the system uncertainties.

The scheduling interval for the ship's power plant is set at 1 hour, and its service load is depicted in Fig. 7(a)-(c). The prediction of cloudy days, outdoor temperature, and photovoltaic power output during ship navigation is shown in Figure 7(d)-(h), where the middle line represents the expected value.

The technical parameters of the power generation equipment, energy conversion units, and energy storage devices in the MESM are presented in Tables II, III, and IV, respectively [6], [33], [34]. Note that without loss of generality, any other data collected from the real world can also be applied.

TABLE II
PARAMETERS OF POWER GENERATION EQUIPMENT

Unit	Ratio	Unit capacity cost($/kW)	Maintenance costs($/kW)	Life cycle(year)
DGs	0.44	870.56	0.0048	15
GT	0.3	965.28	0.0087	15
PV	0.2	625	0.0028	25

TABLE III
PARAMETERS OF ENERGY CONVERSION EQUIPMENT

Unit	Ratio	Unit capacity cost($/kW)	Maintenance costs($/kW)	Life cycle(year)
WHB	0.8	219.86	0.0087	15
AC	1.69	195.55	0.0083	15
EB	0.98	207.78	0.0055	20
EC	3	165.55	0.0044	25

TABLE IV
PARAMETERS OF ENERGY STORAGE

Unit	Ratio	Self-discharging rate	Unit capacity cost($/kWh)	Maintenance costs($/kW)	Life cycle(year)
BS	0.9	0.98	21.67	0.0022	5
TS	0.9	0.97	15.83	0.0025	20

The simulation is conducted on an Intel(R) Core(TM) i5-12400 2.50GHz 64-bit PC with 16G RAM and solved by the Cplex solver via Matlab 2022b platform.

B. Simulation Results

The system's energy scheduling under the worst-case scenario is illustrated in Figure 8.

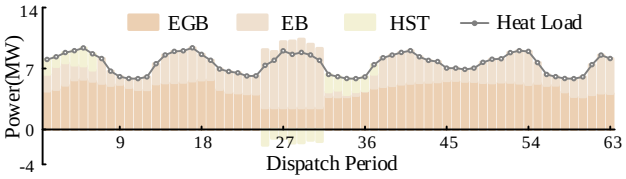

(a). Heat loads balance condition

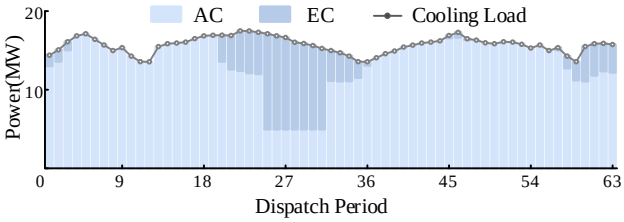

(b). Cooling loads balance condition

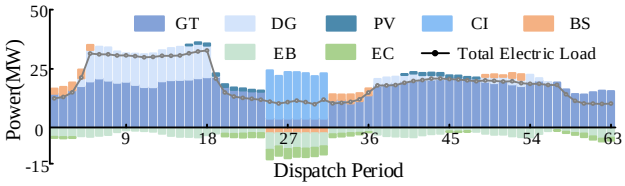

(c). Electric loads balance condition

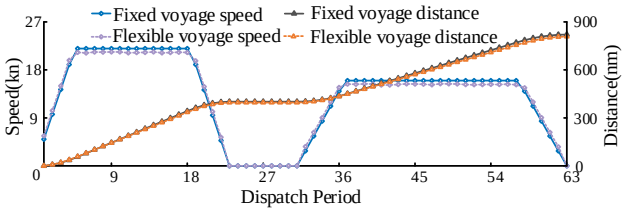

(d). Voyage scheduling condition.

Fig. 8. Diagram of load balancing for each load.

In terms of thermal energy loads, they are satisfied by the AC and WHB systems. The EC and EB, due to their flexible output capabilities, serve as compensatory power sources. Additionally, given the comparatively lower cooling storage efficiency of TS in contrast to the heightened efficiency of EC, TS primarily finds application in the storage and release of thermal energy [Fig.8 (a)-(b)].

Apart from conventional loads and propulsion loads, the electrical system also caters to the electricity demands for refrigeration and heating purposes. Considering the high efficiency of CCHP units, they operate continuously, maintaining minimum power output only during port stays where energy is primarily supplied by shore power (Period: 25-31). DG primarily functions as a compensatory power source during high-speed navigation when the output of the CCHP units is insufficient. Furthermore, both the BT and TS systems store energy during port stays and discharge it during cruising periods. [Fig.8 (c)].

In terms of navigation, both speed and distance exhibit flexibility [Fig. 8(d)], yet remain within defined constraints. Consequently, the propulsion load can be dynamically scheduled to optimize energy usage, thereby ensuring minimal operational costs.

It can be observed that throughout the entire voyage process, the electrical, cooling, and heating loads remain balanced, thus substantiating the effectiveness of the MESM planning methodology.

C. Comparative Simulation

To fully validate the advantages of our method, the following comparison simulations will be conducted:

TABLE V
FOUR METHOD SETTINGS

	Thermal inertia	Ship navigation	RO
Method #1		√	√
Method #2	√		
Method #3	√	√	
Method #4	√	√	√

Method #1: A joint planning method that does not consider thermal inertia but utilizes RO to handle uncertainties in ship operation;

Method #2: A joint planning method that considers thermal inertia but does not consider uncertainties in ship operation;

Method #3: A joint planning method that considers thermal inertia but uses deterministic methods;

Method #4: A joint planning method that considers thermal inertia and utilizes RO to handle uncertainties in ship operation, i.e., our method.

The comparative results are shown in Tables VI and VII.

TABLE VI
COMPARATIVE RESULTS OF DIFFERENT METHODS (ITEMIZED COST).

			Annual operating cost						
	Investment Cost (10^6\$)	Operation cost (10^6\$)	Diesel consumption cost (ton)	Gas consumption cost (ton)	Maintenance costs (10^6\$)	Carbon emissions costs (10^6\$)	Interruption penalty cost (10^6\$)	Unit start-up and shut-down cost (10^6\$)	Health degradation cost (10^6\$)
Method**#1**	65.7112	509.5705	5168	17964	0.8607	11.0557	0	4.2109	0.00907
Method**#2**	58.9197	528.9934	4096	17430	0.8131	10.2377	4.0520	3.9155	0.00933
Method**#3**	59.0657	529.4449	4114	17425	0.8131	10.2451	4.0546	3.9177	0.00934
Method#4	**59.4356**	**469.7359**	**4164**	**17410**	**0.8132**	**10.2649**	**0**	**3.9237**	**0.00955**

TABLE VII
COMPARATIVE RESULTS OF DIFFERENT METHODS

	Total Cost (10^6\$)	NPV (10^6\$)	IRR
Method**#1**	575.2817	63.1491	21.59%
Method**#2**	587.9131	62.7076	21.23%
Method**#3**	588.5106	62.6641	21.20%
Method**#4**	**529.1715**	**66.3102**	**24.37%**

TABLE VIII
CAPACITY CONFIGURATION RESULTS

Item	Method **#1**	Method **#2**	Method **#3**	Method **#4**
DG (kW)	18182	14517	14679	**15083**
GT (kW)	22089	21863	21863	**21863**
WHB (kW)	5848	5787	5787	**5787**
AC (kW)	13666	11800	11800	**11800**
EC (kW)	3628	5317	5317	**5317**
EB (kW)	5054	4351	4351	**4351**
PV (kW)	577	594	601	631
BT (kWh)	5701	5407	5364	**5633**
TS (kW)	1209	2015	2073	**2002**

1) Comparative analysis of ***Method#1*** and ***Method#4***

As shown in Tables VI and VII, the NPV and IRR of Method 1 are significantly lower, reaching only \$63.1491 million and 21.59%, respectively. The primary reason for this difference is that, compared to Method 1, Method 4 achieves reductions of \$6.2756M and \$39.8346M in investment and operational costs, respectively. The simulation results indicate that the proposed approach, which considers system thermal inertia, enhances the flexibility of thermal scheduling and results in greater energy savings. Consequently, the capacity allocation for DG, GT, WHB, AC, and EB in Method 4 is lower than in Method 1, demonstrating the advantage of our approach in leveraging thermal inertia.

In summary, the lower investment and operating costs in Method 4 lead to a higher NPV and IRR than in Method 1, making the planning solution in Method 4 superior. Accounting for system thermal inertia enhances thermal scheduling flexibility and reduces overall costs.

2) Comparative analysis of ***Method#2*** and ***Method#4***

It can be seen from Tables VI and VII that, Method 2 has an NPV and IRR of \$62.7076M and 21.23%, respectively, both lower than those achieved by the proposed method. This discrepancy is primarily due to Method 4's consideration of actual operating conditions, where the uncertain effects of wind and wave forces on vessel operation are incorporated, requiring additional energy to ensure safe navigation. This factor increased DG capacity allocation, leading to a higher investment cost in Method 4. However, operational costs in Method 4 are 11.2% lower than in Method 2, mainly because Method 2 incurs \$4.052M more in interruption penalty costs, suggesting it is less adaptable to varying operational scenarios, whereas the proposed method effectively addresses such uncertainties.

In conclusion, due to the significantly lower operational costs, Method 4 yields a higher NPV and IRR than Method 2. The planning approach in Method 4 accounts for actual vessel operating conditions, aligning more closely with real-world scenarios and demonstrating greater adaptability across different scenarios.

3) Comparative analysis of ***Method#3*** and ***Method#4***

As shown in Tables VI and VII, Method 3 achieves an NPV of \$62.6641M and an IRR of 21.20%. The primary reason for this outcome is that the robust optimization approach in Method 4 makes capacity allocation decisions under worst-case conditions, resulting in a 404 kW increase in DG capacity to address the worst-case uncertainties impacting vessel speed, thereby ensuring safe navigation. Consequently, Method 3 incurs an additional \$4.0546M in interruption penalty costs, indicating that in certain situations, the deterministic approach in Method 3 proves infeasible due to the need to curtail loads to maintain energy balance. In contrast, the proposed method can accommodate all scenarios without load shedding, verifying the robustness of our solution in addressing uncertainties.

In summary, the higher operational costs of Method 3 lead to lower NPV and IRR values compared to Method 4. The robust optimization approach proposed in this study not only

ensures reliable vessel operation under diverse scenarios but also reduces costs and increases profitability, making it a more practical solution than deterministic methods.

D. Sensitivity Analysis

To further investigate the effectiveness and robustness of the proposed method, this study introduces two scenarios with varying levels of uncertainty, denoted as "case1" and "case2" representing low and high uncertainty sources, respectively. The uncertainty values for these scenarios are depicted in Fig9 and Fig10.

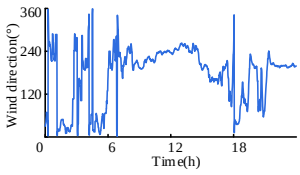

(a)Wind direction

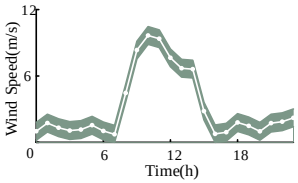

(b)Wind speed prediction

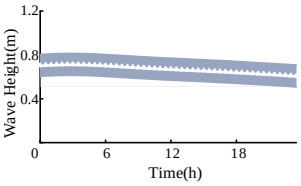

(c) Wave height prediction

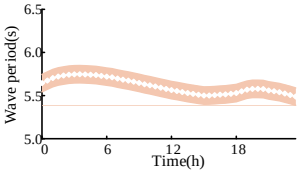

(d)Wave period prediction

Fig. 9. Interval predictions for uncertainties in Case 1.

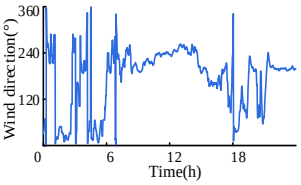

(a)Wind direction

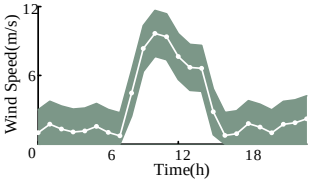

(b)Wind speed prediction

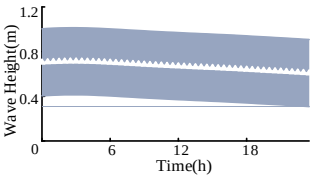

(c) Wave height prediction

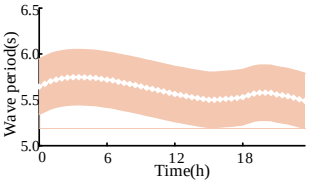

(d)Wave period prediction

Fig. 10. Interval predictions for uncertainties in Case 2.

TABLE IX
PLANNING RESULTS OF EACH CASE 1 AND CASE 2 (ITEMIZED COST)

	INVESTMENT COST (10^6\$)	Operation cost (10^6\$)	diesel consumption (ton)	Gas consumption (ton)	Maintenance costs (10^6\$)	Carbon emissions costs (10^6\$)	Interruption penalty cost (10^6\$)	Unit start-up and shut-down cost (10^6\$)	Health degradation cost (10^6\$)
Case 1	59.1451	468.8680	4125	17421	0.8131	10.2494	0	3.9190	0.00906
Case 2	59.6033	470.3368	4191	17403	0.8132	10.2756	0	3.9270	0.00924

TABLE X
PLANNING RESULTS OF EACH CASE 1 AND CASE 2

	Total Cost (10^6\$)	NPV (10^6\$)	IRR
Case 1	528.0131	66.3955	24.45%
Case 2	529.9401	66.2548	24.32%

TABLE XI.
CAPACITY CONFIGURATION RESULTS

	Case 1	**Case 2**
DG (kW)	14771	15284
GT (kW)	21863	21863
WHB (kW)	5787	5787
AC (kW)	11800	11800
EC (kW)	5317	5317
EB (kW)	4352	4352
PV (kW)	617	648
BT (kWh)	5407	5501
TS (kW)	2015	2852

From the sensitivity analysis results outlined above, the following observations can be made:

1) The robustness of the RO method is confirmed, ensuring the safe navigation of vessels under varying levels of uncertainty.

2) The RO method demonstrates effectiveness in handling uncertainty. As indicated in Tab. VIII, there are no infeasible scenarios during operation, regardless of whether uncertainty levels are high or low.

3) For the different scenarios under the RO method, total costs increase with increasing uncertainty levels, validating the ability of the RO approach to identify worst-case uncertainty realizations.

VI. CONCLUSION

This paper proposes a two-stage coordinated joint planning method for MESM considering uncertainties and system thermal inertia. Simulation results reveal several key findings:

1) The MESM planning method has proved to be rational and effective, yielding planning outcomes that ensure economic and safe vessel operation.

2) In the heating/cooling system, the consideration of thermal inertia, along with the expansion of the acceptable temperature range, further explores the system's adjustable resources, resulting in a lower total cost.

3) Incorporating the effects of wind and waves into the ship's navigation process brings the model closer to real-world conditions, thereby enhancing the stability and safety of ship operations.

4) The RO method provides robustness for the MESM operation against uncertainties.

In summary, the proposed MESM joint planning method can achieve lower operating costs while enhancing system stability and safety.

In future work, we will focus primarily on further in-depth studies of more precise multi-energy coupling models and ship route planning and operation. Specific details are as follows:

1) Future multi-energy coupling models will incorporate

more accurate photovoltaic output and storage degradation.

2) Ship route flexibility significantly affects economic efficiency, so route management will be a focus of upcoming work.

3) Machine learning can use historical data to enable online operation and intelligent planning, and will be explored in future studies on ship planning and operation.

REFERENCES

[1] Y. Tao, J. Qiu, S. Lai, X. Sun and J. Zhao, "Flexible Voyage Scheduling and Coordinated Energy Management Strategy of All-Electric Ships and Seaport Microgrid," *IEEE Trans. Intell. Transp. Syst*, vol. 24, no. 3, pp. 3211-3222, March 2023.

[2] Z. Fei, H. Yang, L. Du, J. M. Guerrero, K. Meng and Z. Li, "Two-Stage Coordinated Operation of A Green Multi-Energy Ship Microgrid With Underwater Radiated Noise by Distributed Stochastic Approach," *IEEE Trans. Smart Grid*, early access, Oct. 17, 2024, doi: 10.1109/TSG.2024.3482980.

[3] S. Wen, X. Jin, Y. Zheng and M. Wang, "Probabilistic Coordination of Optimal Power Management and Voyage Scheduling for All-Electric Ships," *IEEE Trans. Transp. Electrif.*, vol. 10, no. 2, pp. 3661-3669, June 2024

[4] A. Lin, S. Wen, M. Zhu, Z. Ding and T. Ding, "Joint Optimal Energy Management and Voyage Scheduling for Economic and Resilient Operation of All-Electric Ships Considering Safe Return," *IEEE Trans. Ind. Appl.*, vol. 59, no. 5, pp. 5304-5313, Sept.-Oct. 2023

[5] A. Lin, S. Wen, M. Zhu and X. Cai, "Risk-Aware Coordination of Logistics Scheduling and Energy Management for Maritime Mobile Microgrid Clusters," *IEEE T. Intell. Veh.*, vol. 9, no. 1, pp. 752-763, Jan. 2024

[6] S. Wen, T. Zhao, Y. Tang, Y. Xu, M. Zhu, S. Fang and Z. Ding, "Coordinated Optimal Energy Management and Voyage Scheduling for All-Electric Ships Based on Predicted Shore-Side Electricity Price," *IEEE Trans. Ind. Appl*, vol. 57, no. 1, pp. 139-148, Jan.-Feb. 2021

[7] S. Wen, T. Zhao, Y. Tang, Y. Xu, S. Fang, M. Zhu and Z. Ding, "Joint Energy Management and Voyage Scheduling for All-Electric Ships Using Dynamic Real-Time Electricity Price of Onshore Power," *2020 IEEE/IAS 56th Industrial and Commercial Power Systems Technical Conference (I&CPS)*, Las Vegas, NV, USA, 2020, pp. 1-8

[8] T. Zhao, J. Qiu, S. Wen and M. Zhu, "Efficient Onboard Energy Storage System Sizing for All-Electric Ship Microgrids Via Optimized Navigation Routing Under Onshore Uncertainties," *IEEE Trans. Ind. Appl*, vol. 58, no. 2, pp. 1664-1674, March-April 2022

[9] R. Yang, H. Wei and L. Wang, "Research on Energy Regulation and Optimal Operation Strategy of Multi-energy Ship Power Station Based on Improved Particle Swarm Algorithm," *2021 IEEE 5th Advanced Information Technology, Electronic and Automation Control Conference (IAEAC)*, Chongqing, China, 2021, pp. 294-298

[10] S. Fang, Y. Xu, Z. Li, Z. Ding, L. Liu and H. Wang, "Optimal Sizing of Shipboard Carbon Capture System for Maritime Greenhouse Emission Control," *IEEE Trans. Ind. Appl*, vol. 55, no. 6, pp. 5543-5553, Nov.-Dec. 2019

[11] M. Acanfora, F. Balsamo, M. Fantauzzi, D. Lauria and D. Proto, "Design of an electrical energy storage system for hybrid diesel electric ship propulsion aimed at load levelling in irregular wave conditions." *Appl. Energy*, vol. 350, p. 121728, 2023.

[12] F. Hardan and P. Tricoli, "Optimization and Control of Electric Ship Microgrids With Short-Term Energy Storage Systems," *IEEE Trans. Transp. Electrif,* vol. 10, no. 3, pp. 4734-4745, Sept. 2024, doi: 10.1109/TTE.2023.3326355.

[13] C. Yang, A. Li, W. Han, Z. Wu, S. Wang, Y. Jia, J. Li, Y. Min, and Y. Yuan, "Application of composite energy storage device in ship electric propulsion system," *J. Mar. Sci. Technol.-Taiwan,* vol. 27, no. 2, pp. 907–915, 2022.

[14] Z. Li, Y. Xu, S. Fang, X. Zheng and X. Feng, "Robust Coordination of a Hybrid AC/DC Multi-Energy Ship Microgrid With Flexible Voyage and Thermal Loads," *IEEE Trans. Smart Grid*, vol. 11, no. 4, pp. 2782-2793, July 2020.

[15] Z. Li and Y. Xu, "Temporally-coordinated optimal operation of a multi-energy microgrid under diverse uncertainties," *Appl. Energy*, vol. 240,no. 1, pp. 719–729, 2019.

[16] Z. Li, Y. Xu, L. Wu and X. Zheng "A risk-averse adaptively stochastic optimization method for multi-energy ship operation under diverse uncertainties." *IEEE Trans. Power Syst*, vol. 36, no. 3, pp. 2149-2161, May 2021.

[17] Prékopa, András. Stochastic programming. Vol. 324. *Springer Science & Business Media*, 2013.

[18] W. Sun, Q. Wang, Y. Ye, and Y. Tang, "Unified modelling of gas and thermal inertia for integrated energy system and its application to multitype reserve procurement," *Appl. Energy*, vol. 305, Art. no. 117963, 2022.

[19] M. Voss, J. F. Heinekamp, S. Krutzsch, F. Sick, S. Albayrak and K. Strunz, "Generalized Additive Modeling of Building Inertia Thermal Energy Storage for Integration Into Smart Grid Control," *IEEE Access*, vol. 9, pp. 71699-71711, 2021

[20] Y. Chen, Y. Xu, Z. Li, and X. Feng. "Optimally coordinated dispatch of combined-heat-and-electrical network with demand response, " *IET Renew. Power. Gen.,* vol. 13, no. 11, pp. 2216-2225, 2019.

[21] C. Zhang, Y. Xu and Z. Y. Dong, "Robustly Coordinated Operation of a Multi-Energy Micro-Grid in Grid-Connected and Islanded Modes Under Uncertainties," *IEEE Trans. Sustain. Energy*, vol. 11, no. 2, pp. 640-651, April 2020.

[22] N. S. Isa, M. F. Akhir, I. Khalil, P. H. Kok, and N. H. Roseli, "Seasonal characteristics of the sea surface temperature and sea surface currents of the Strait of Malacca and Andaman Sea," *J. Sustain. Sci. Manage.*, vol. 15, no. 4, pp. 66-77, 2020.

[23] M. Fujita, F. Kimura, and M. Yoshizaki, "Morning precipitation peak over the Strait of Malacca under a calm condition," *Mon. Weather Rev.* vol. 138, no. 4, pp. 1474-1486, 2010.

[24] M. Kim, O. Hizir, O. Turan, S. Day, and A. Incecik, "Estimation of added resistance and ship speed loss in a seaway," *Ocean Eng*., vol. 141, pp. 465–476. 2017

[25] Z. Li and Y. Xu, "Optimal coordinated energy dispatch of a multi-energy microgrid in grid-connected and islanded modes." *Appl. Energy, vol.* 210, pp. 974-986, 2018.

[26] F. D. Kanellos, A. Anvari-Moghaddam, and J. M. Guerrero, "A cost-effective and emission-aware power management system for ships with integrated full electric propulsion," *Electr. Pow. Syst. Res.*, vol. 150, pp. 63-75, 2017.

[27] A. Hussain, Q. S. Khalid, M. Alkahtani, and A. M. Khan, "A Mathematical Model for Optimizing NPV and Greenhouse Gases for Construction Projects Under Carbon Emissions Constraints," *IEEE Access,* vol. 12, pp. 31875-31891, 2024.

[28] P. J. Barry and L. J. Robison, "Economic rates of return and investment analysis". *Eng. Econ.,* vol. 59, no. 3, pp. 231-236, 2014.

[29] "ROYAL CARIBBEAN GROUP REPORTS 2023 RESULTS AND EX PECTS RECORD EARNINGS IN 2024 ON STRONG DEMAND," *Ro yal Caribbean Group*, Feb. 1, 2024. [Online]. Available: https://www.rclinvestor.com/press-releases/release/?id=1687. Accessed: Oct. 30, 2024.

[30] B. Zeng and L. Zhao, "Solving two-stage robust optimization problems using a column-and-constraint generation method", *Oper. Res. Lett.,* vol. 41, no. 5, pp. 457-461, 2013.

[31] H. D. Chiang, Z. Y. Wang, and L. Zeng, "Dynamic Relationship Between KKT Saddle Solutions and Optimal Solutions in AC OPF Problems," *IEEE Trans. Power Syst.*, vol. 39, no. 1, pp. 1637-1646, 2023.

[32] H. Fazhan, K. Waiho, M. F. D. Azri, I. Al-Hafiz, W. I. W. Norfaizza, F. H. Megat, and M. Ikhwanuddin, "Sympatric occurrence and population dynamics of Scylla spp. in equatorial climate: effects of rainfall, temperature and lunar phase." *Estuar. Coast. Shelf Sci.* vol. 198, pp. 299-310, 2017.

[33] C. Wan, Z. Xu, P. Pinson, Z. Y. Dong, and K. P. Wong, "Probabilistic forecasting of wind power generation using extreme learning machine, "*IEEE Trans. Power Syst*., vol. 29, no. 3, pp. 1033–1044, May 2014.

[34] G. Theotokatos, A. Rentizelas, C. Guan, and I. Ancic, "Waste heat recovery steam systems techno-economic and environmental investigation for ocean-going vessels considering actual operating profiles." *J. Clean Prod.* vol. 267, pp. 121837, 2020.

Nan Yang (Senior Member, IEEE) received the B.S. degree in electrical engineering from Taiyuan University of Technology, Taiyuan, China, in 2009, and the Ph.D. degree in electrical engineering from Wuhan University, Wuhan, China, in 2014. He worked as a Visiting Scholar with the Stevens Institute of Technology, Hoboken, NJ, USA during 2019-2020. He is currently a professor at the College of Electrical Engineering and New Energy, China Three Gorges University. His major research interests include power dispatching automation of new energy sources, artificial intelligence,

planning and operation of power systems, operation and control of microgrid, and active distribution networks.

Guobin Xu received the B.S. degree in automation from North China Electric Power University, Beijing, China, in 2022. He is currently pursuing the M.S. degree with the College of Electrical Engineering and New Energy, China Three Gorges University, Yichang, China. His primary research interests focus on the operation and planning of ship energy systems.

Zhineng Fei (Student Member, IEEE) received his M.S. degree in Management Science and Engineering from Hefei University of Technology, Hefei, China, in 2023. He is currently pursuing a Ph.D. in Electrical Engineering at Aalto University, Espoo, Finland. His research interests include ship and building energy systems and uncertainty handling.

Zhengmao Li (Member, IEEE) received his Ph.D. degree from the School of Electrical and Electronic Engineering, Nanyang Technological University, Singapore, in 2020. He was a Research Fellow at Stevens Institute of Technology, USA (2019–2021), and Nanyang Technological University and Singapore ETH Center (2021–2023). In 2023, he joined Aalto University as an Assistant Professor. His research interests include renewable energy integration, microgrids, and multi-energy systems.

Liang Du (Senior Member, IEEE) received the Ph.D. in electrical engineering from the Georgia Institute of Technology, Atlanta, GA, USA, in 2013. He was a Research Intern with Eaton Corporation Innovation Center, Mitsubishi Electric Research Labs, and Philips Research N.A (2011-2013), and an Electrical Engineer with Schlumberger, Sugar Land, TX, USA (2013-2017). He is currently an Assistant Professor in the Department of Electrical and Computer Engineering, Temple University, Philadelphia, PA, USA. He is an Associate Editor for IEEE Transactions on Sustainable Energy and IEEE Transactions on Transportation Electrification.

Josep M. Guerrero (Fellow, IEEE) received the B.S. degree in telecommunications engineering, the M.S. degree in electronics engineering, and the Ph.D. degree in power electronics from the Technical University of Catalonia, Barcelona, Spain, in 1997, 2000, and 2003, respectively. He has been a Full Professor with AAU Energy, Aalborg University, Denmark, since 2011 and became an ICREA Research Professor at the Technical University of Catalonia in 2023. His research interests include photovoltaics, wind energy conversion, uninterruptible power supplies, storage energy systems, and microgrids.

Yuehua Huang (Member, IEEE) received the B.S. degree in electrical machinery from Huazhong University of Science and Technology, Wuhan, China, in 1994, and the Ph.D. degree in Control Science and Engineering from Huazhong University of Science and Technology, Wuhan, China, in 2013. He is currently a professor at the College of Electrical Engineering and New Energy, China Three Gorges University. His major research interests include new energy microgrid technology and intelligent distribution network.

Jing Yan received the M.S. degree in electrical engineering from Wuhan University, in 2013. He is currently a Senior Engineer with the Hubei Economic and Technological Research Institute of the State Grid. His main research interests include artificial intelligence and planning and operation of power systems.

Chao Xing (Member, IEEE) received an M.S. degree from Wuhan University, Wuhan, China, in 2011. He is currently a senior engineer of the Department of Electric Power Research Institute of Yunnan Power Grid Co., Ltd., Kunming, China. His research interests include DC transmission control protection and test technology.

Zhenhua Li (Senior Member, IEEE) received the B.Sc. degree in biotechnology and the M.Sc. degree in electric engineering from the Huazhong University of Science and Technology, Wuhan, China, in 2008 and 2011, respectively, and the Ph.D. degree in electric engineering from same University, in 2014.He is currently an Professor with China Three Gorges University, Yichang, China. His current research interests include the condition monitoring of aircraft electric power source, electromagnetic compatibility, energy managements, and fault diagnosis.